

DNAJB6 isoform specific knockdown: Therapeutic potential for limb girdle muscular dystrophy D1

Andrew R. Findlay,¹ May M. Paing,¹ Jil A. Daw,¹ Meade Haller,¹ Rocio Bengoechea,¹ Sara K. Pittman,¹ Shan Li,² Feng Wang,² Timothy M. Miller,¹ Heather L. True,³ Tsui-Fen Chou,² and Conrad C. Weihl¹

¹Department of Neurology, Neuromuscular Division, Washington University School of Medicine, Saint Louis, MO 63110, USA; ²Division of Biology and Biological Engineering, California Institute of Technology, Pasadena, CA 91125, USA; ³Department of Cell Biology and Physiology, Washington University School of Medicine, 660 South Euclid Avenue, Campus Box 8228, St. Louis, MO 63110, USA

Dominant missense mutations in DNAJB6, a co-chaperone of HSP70, cause limb girdle muscular dystrophy (LGMD) D1. No treatments are currently available. Two isoforms exist, DNAJB6a and DNAJB6b, each with distinct localizations in muscle. Mutations reside in both isoforms, yet evidence suggests that DNAJB6b is primarily responsible for disease pathogenesis. Knockdown treatment strategies involving both isoforms carry risk, as DNAJB6 knockout is embryonic lethal. We therefore developed an isoform-specific knockdown approach using morpholinos. Selective reduction of each isoform was achieved *in vitro* in primary mouse myotubes and human LGMDD1 myoblasts, as well as *in vivo* in mouse skeletal muscle. To assess isoform specific knockdown in LGMDD1, we created primary myotube cultures from a knockin LGMDD1 mouse model. Using mass spectrometry, we identified an LGMDD1 protein signature related to protein homeostasis and myofibrillar structure. Selective reduction of DNAJB6b levels in LGMDD1 myotubes corrected much of the proteomic disease signature toward wild type levels. Additional *in vivo* functional data is required to determine if selective reduction of DNAJB6b is a viable therapeutic target for LGMDD1.

INTRODUCTION

Limb girdle muscular dystrophy type-D1 (LGMDD1) is caused by dominantly inherited mutations in *DNAJB6*. LGMDD1 patients have a wide age range of onset and may have either a proximal or distal predominant pattern of weakness.¹ Muscle biopsies demonstrate a vacuolar myopathy with aggregates, as well as myofibrillar abnormalities involving the Z disc. No treatments are available. The standard of care is supportive in nature. Since its discovery in 2012, mutations in *DNAJB6* are the most common cause of dominantly inherited LGMD.²

DNAJB6 is a ubiquitously transcribed co-chaperone of HSP70 with a wide array of functions. It acts as a tumor suppressor, prevents aggregation of polyglutamine-containing proteins, and plays a role in viral replication cycles, just to name a few.³ While dominantly inherited mutations in *DNAJB6* cause a degenerative disorder of skeletal muscle, the absence of *DNAJB6* manifests differently and is embryonic lethal in mice. This has been attributed to aggregation of a couple of

DNAJB6's client proteins, keratin 8/18, within chorionic trophoblast cells, causing failure of chorioallantoic attachment during placental development.⁴ DNAJB6's role in muscle is thought to be related to protein homeostasis, but how dominantly inherited mutations in a ubiquitously expressed co-chaperone cause selective pathology in skeletal muscle is unknown.

DNAJB6 has two key isoforms—DNAJB6a a large nuclear predominant isoform, as well as DNAJB6b, a shorter isoform that localizes to sarcomeric structures in muscle, a key site of pathology seen in muscle biopsies from patients.⁵ Mutations associated with LGMDD1 are located in regions of *DNAJB6* that affect both isoforms. However, several lines of evidence suggest that the B isoform preferentially contributes to disease pathogenesis.^{5,6} Zebrafish injected with mutant human *DNAJB6b* mRNA resulted in myofibrillar abnormalities, whereas mutant *DNAJB6a* mRNA did not.⁶ Additionally, transgenic mice overexpressing mutant human DNAJB6b in muscle caused a myopathy, whereas mice overexpressing mutant DNAJB6a were not different from controls.⁵ However, there is some evidence suggesting that DNAJB6a is not completely dispensable in muscle; a patient with a myofibrillar myopathy was found to have recessively inherited frameshift mutations selectively affecting DNAJB6a expression.⁷ Overall, each isoform's role in muscle and their contribution to LGMDD1 pathogenesis remains unclear.^{5,6,8–12}

Although gene knockdown is a common approach for treating dominantly inherited disorders, this approach may be deleterious in LGMDD1 based on DNAJB6 knockout data in cells and mice. However, haploinsufficiency may be tolerated; human mutation databases such as gnomAD contain frameshift and nonsense mutations scattered throughout DNAJB6 in presumably healthy patients.⁴ Recently, DNAJB6 haploinsufficiency was associated with a sick sinus syndrome phenotype in mice with no structural cardiac changes.¹³

Received 17 November 2022; accepted 10 May 2023;
<https://doi.org/10.1016/j.omtn.2023.05.017>

Correspondence: Andrew R. Findlay, Department of Neurology, Neuromuscular Division, Washington University School of Medicine, Saint Louis, MO 63110, USA.
E-mail: arfindlay@wustl.edu



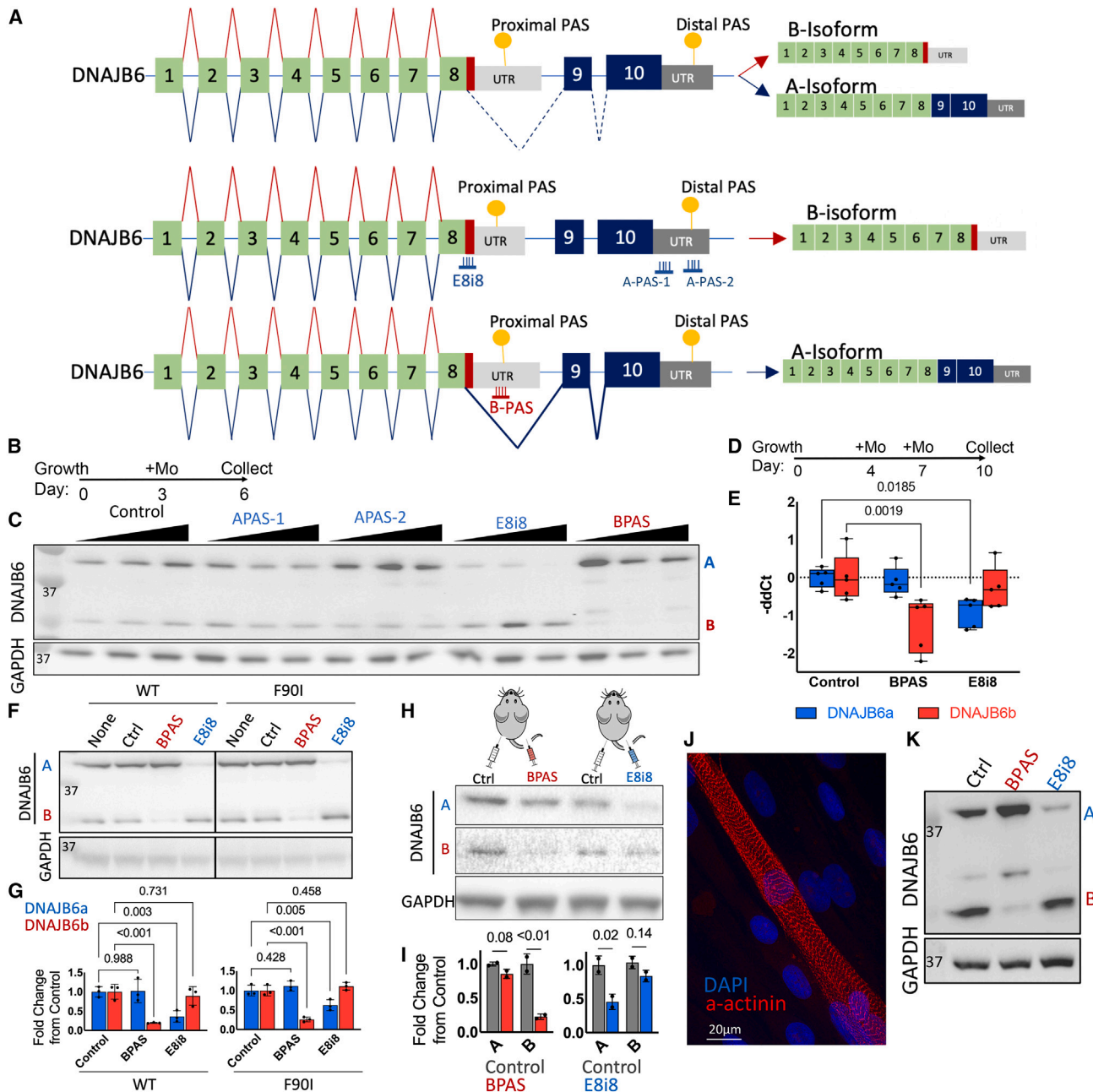


Figure 1. Selective DNAJB6 isoform knockdown *in vitro* in primary mouse myotubes and primary human myoblasts and *in vivo* in mouse skeletal muscle (A) Map of *DNAJB6* gene structure and transcripts generated by competition between alternative splicing and polyadenylation. Morpholinos designed to selectively reduce *DNAJB6b* transcript (BPAS) targets the proximal PAS, sterically blocking this sequence, in theory, preventing its polyadenylation. Morpholinos designed to selectively reduce *DNAJB6a* transcript by targeting the distal PAS (A-PAS1, A-PAS2), or by blocking intron 8 splicing (E8i8). (B) Culture and treatment timeline for screening morpholinos (Mo) in primary mouse myotubes. (C) Western blot of lysates from primary mouse myotubes treated with morpholinos to achieve isoform specific knockdown. BPAS and E8i8 appear to result in a dose dependent reduction of their intended targets. Morpholino doses: 2.5 µM, 5 µM, and 10 µM. (D) Culture and treatment timeline for optimizing *DNAJB6* isoform knockdown in mature myotubes. Morpholino doses: 5 µM (control [ctrl], E8i8), 2.5 µM (BPAS). To achieve more comparable levels of isoform-specific knockdown, a lower dose of BPAS was used. (E) Boxplots of *DNAJB6* isoform-specific real-time qPCR (RT-qPCR) of primary mouse myotubes treated with control, BPAS, or E8i8 morpholinos. BPAS results in significant reduction of only the B isoform transcript, whereas E8i8 causes a significant reduction of only the A isoform transcript. Dots represent experimental replicates (n = 5). Each experimental replicate was generated from 3 technical replicates. Whiskers represent the range, the upper and lower borders of the box represent the first (25%) and third quartiles (75%), and the horizontal line is the median. One-way ANOVA with Tukey's post-hoc test comparing BPAS or E8i8 treatment to control. Only significant comparisons are shown. (F) Representative Western blot of lysates from primary mouse myotubes treated with optimized culture and morpholino

(legend continued on next page)

Therapeutic approaches will, therefore, need to address the dominant mechanism of DNAJB6 mutations, but avoid the potential deleterious effects of complete knockdown.

Given that the B isoform seems to preferentially contribute to disease pathogenesis, and the dominant disease mechanism in LGMDD1, selective reduction of DNAJB6b levels could be a potential therapeutic target. The mechanism governing DNAJB6 isoform expression was recently characterized and involves splicing-coupled alternative polyadenylation, leading to the mutually exclusive usage of two terminal exons.¹⁴ Production of the short B isoform depends on use of a weak proximal polyadenylation signal (PAS) and a lack of intron 8 splicing. This is regulated by CSTF64, a polyadenylation factor, which binds to and promotes the use of the weak proximal PAS within intron 8. When bound, CSTF64 competitively inhibits splicing machinery from binding to intron 8, preventing its splicing. Low CSTF64 levels allow for splicing machinery to bind and excise intron 8, leading to the use of the strong distal PAS downstream of exon 10, and production of the large A isoform. In this work we designed morpholinos, a type of antisense oligonucleotide (ASO), to achieve DNAJB6 isoform-specific knockdown and assessed the therapeutic potential of selective DNAJB6b reduction in LGMDD1.

RESULTS

We developed two strategies using morpholinos to prevent the production of DNAJB6a: blocking DNAJB6a's PAS, theoretically destabilizing DNAJB6a mRNA (A-PAS-1, A-PAS-2), or blocking intron 8 splicing (E8i8), to prevent DNAJB6a mRNA production. Selectively targeting DNAJB6b is more difficult; it has no unique sequence compared with DNAJB6a at the DNA or pre-mRNA level. The only sequence unique to the DNAJB6b isoform occurs at the mRNA level and includes 35 coding bases and the 3' UTR (Figure 1A).¹⁴ We, therefore, designed a morpholino (BPAS) targeting DNAJB6b's PAS, theoretically impairing its polyadenylation and destabilizing the transcript. As intron 8 splicing is competitively coupled to alternative polyadenylation, blocking this proximal PAS may promote intron 8 splicing, preventing B isoform expression even further.¹⁴

Morpholinos designed for selective reduction of each DNAJB6 isoform were first screened using C57/B6 primary myoblasts differentiated into myotubes. Myoblasts were grown for 3 days to near confluency before the media was changed and morpholinos were added (Figure 1B). Morpholinos were taken up by gymnosis because of the presence of an octaguanidine dendrimer moiety that improves

uptake. Myotubes formed over the next 3 days and cells were collected for western blot (Figure 1C). The E8i8 morpholino effectively reduced the DNAJB6a isoform and BPAS selectively reduced the DNAJB6b isoform relative to myotubes treated with a control morpholino. Morpholinos targeting the A isoform's PAS (A-PAS-1, A-PAS-2) were not effective (Figure 1C).

We optimized our protocol to maximize both isoform-specific knockdown and myotube maturity (Figure 1D). Selective reduction of each isoform was detected at both the RNA and protein levels (Figures 1E–1G). In certain instances, after E8i8 treatment we noted an increase in the B isoform and, after BPAS treatment, we noted increased A isoform levels (Figure 1C).

We previously created a knockin LGMDD1 mouse model with a heterozygous p.F90I mutation (F90I^{+/-}) (orthologous to human p.F89I).⁸ These mice develop a myopathic phenotype by at least 1 year of age.⁸ Using the same differentiation and morpholino protocol described above, E8i8 and BPAS treatments were effective in primary myotube cultures from these F90I^{+/-} mice (Figures 1F and 1G).

We conducted preliminary *in vivo* testing in C57/B6 mice using intramuscular (IM) tibialis anterior (TA) injections and collected muscle 4 days later. Mice received control morpholino in one leg and either BPAS or E8i8 in the other (Figure 1H). Western blot of skeletal muscle lysates demonstrated BPAS and E8i8 are capable of selective isoform reduction at the protein level *in vivo* (Figures 1H and 1I).

To test feasibility in a human model of disease, we isolated primary myoblasts from skeletal muscle biopsies of LGMDD1 patients. These myoblasts readily differentiate into myotubes with sarcomeric structures (Figure 1J). Treatment of LGMDD1 myoblasts containing a p.F89I mutation with BPAS or E8i8 for 3 days also achieved the intended isoform specific reductions at the protein level (Figure 1K).

We next wondered how isoform-specific knockdown might impact an LGMDD1 disease model. We first assessed for any baseline differences between primary myoblasts isolated and cultured from wild-type (WT) and F90I^{+/-} mice. We found no differences in myoblast proliferation rates (Figure 2A), their ability to form myotubes, or their myofibrillar structure as shown by alpha actinin staining (Figures 2B and 2C). Although there were no obvious phenotypic abnormalities in the LGMDD1 primary mouse myotube cultures, this could be related to LGMDD1 being a degenerative disorder of mature skeletal

treatment timeline. (G) Quantitation of western blot. (F) Dots represent experimental replicates (n = 3). Results are presented as mean ± SD. One-way ANOVA with Tukey's post hoc test was used to compare BPAS or E8i8 treatment's impact on DNAJB6a and DNAJB6b levels vs. control. (H) Western blot of skeletal muscle lysates from C57/B6 mice 4 days after IM injection of BPAS or E8i8 into TA of one leg, and control morpholino in the contralateral leg; 10 µg morpholino per leg. The DNAJB6 membrane was split between DNAJB6a and DNAJB6b to develop separately because of the large excess of DNAJB6a relative to DNAJB6b in mature skeletal muscle. (I) Quantitation of Western blot 1H. Dots represent experimental replicates (n = 2). Results are presented as mean ± SD. One-way ANOVA with Tukey's post hoc test was used to compare BPAS or E8i8 treatment's impact on DNAJB6a and DNAJB6b levels vs. control. (J) Primary myoblasts isolated from human LGMDD1 muscle biopsy (p.F89I), differentiated into myotubes, and stained for alpha-actinin (red) and nuclei (blue). Mature myotubes with well-formed sarcomeres are present. (K) Western blot of lysates from LGMDD1 primary human myoblasts treated with morpholinos for 3 days demonstrating effective isoform-specific reduction with BPAS and E8i8.

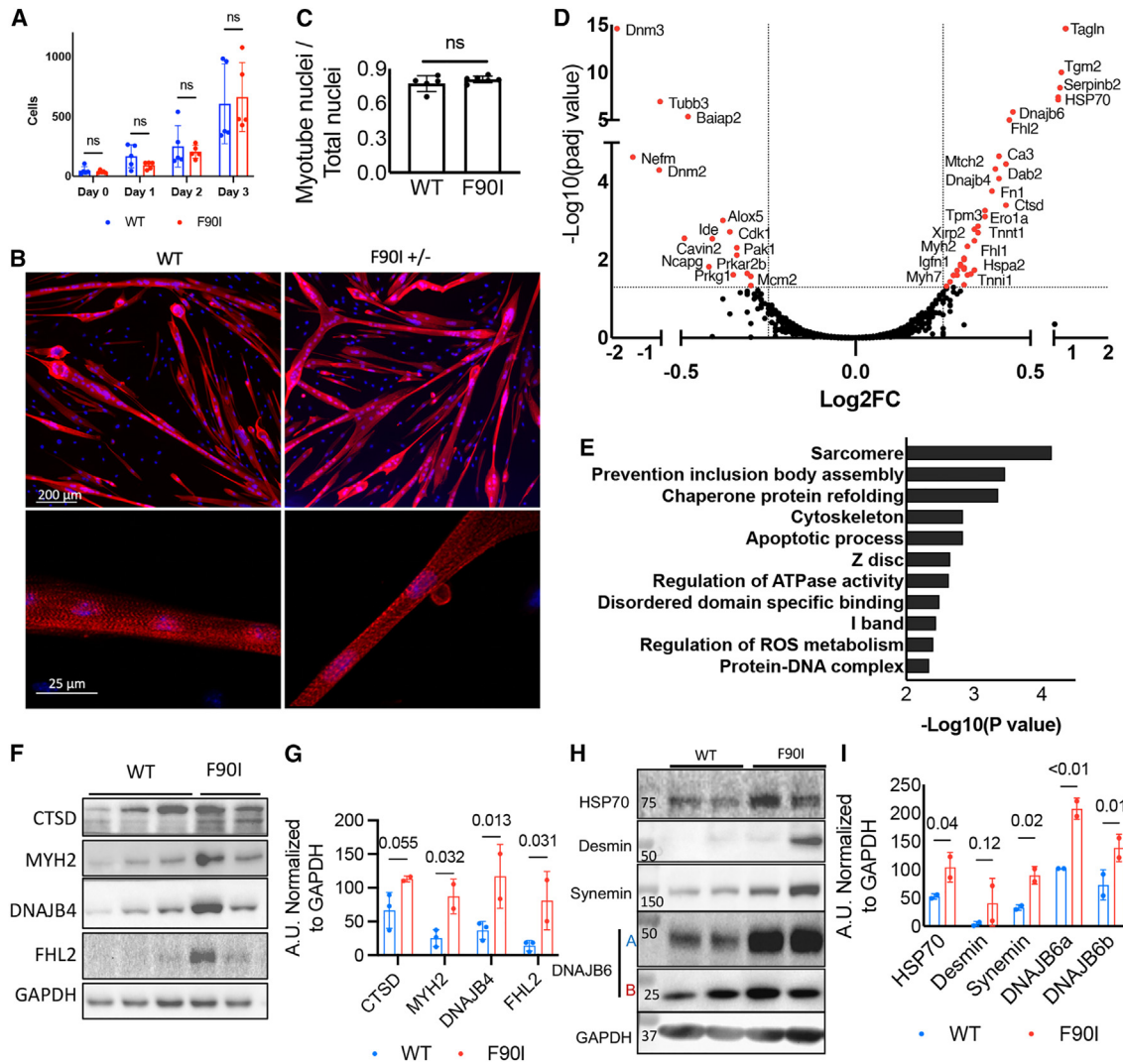


Figure 2. LGMDD1 proteomic signature identifies proteins involved in myofibrillar structure and protein homeostasis in primary mouse myotubes and skeletal muscle

(A) Quantitation of primary myoblast proliferation from F90I^{+/-} and WT mice shows no significant differences. Myoblasts were plated at equal densities, collected at the indicated time points, and stained with DAPI. Results presented as mean ± SD. Dots represent experimental replicates (n = 5). Statistical comparisons made via two-way ANOVA with a Bonferroni post hoc test. (B) Primary myotubes at day 3 of differentiation from F90I^{+/-} and WT mice develop multinucleated myotubes. (Bottom) Higher magnification demonstrating well formed sarcomeric structures. Alpha-actinin (red) and DAPI (blue). (C) Quantitation of myotube nuclei/total nuclei shows no difference between WT and LGMDD1 cell lines. Results presented as mean ± SD. Dots represent experimental replicates (n = 5). Two-tailed, unpaired Student's t test. (D) Volcano plot of mass spectrometry data comparing F90I^{+/-} with WT myotubes (n = 3 experimental replicates). Log₂ fold change (log₂fc) ratio is F90I/WT. Proteins with significantly altered abundances are highlighted in red. (E) Ontological analysis of proteins identified to have altered abundances in F90I^{+/-} myotubes. (F) Western blot validation of several proteins identified in (D) with significantly altered abundances. Each lane is lysate from an experimental replicate of the mass spectrometry experiment. The third F90I^{+/-} replicate is not shown due to absence of GAPDH signal. (G) Quantitation of Western blot (F). Data are presented as mean ± SD. Dots represent experimental replicates from (F). (H) Western blot of skeletal muscle lysates (TA) from F90I^{+/-} mice (n = 2) and WT controls (n = 2) at 2 months of age (the same age at which primary myoblasts were isolated). Protein homeostasis proteins: DNAJB6 and HSP70. Myofibrillar proteins: desmin and synemin. (I) Quantitation of Western blot (H). Data presented as mean ± SD. Dots represent experimental replicates from (H).

muscle, not a condition with congenital onset related to dysfunctional muscle formation.

To better characterize a monitorable disease phenotype in LGMDD1 primary myotubes, we sought to use a broad “omic”--

based approach as DNAJB6 has many functions, and it is unclear which of those functions are impacted by disease mutations.³ We, therefore, decided to use mass spectrometry as chaperone dysfunction might be most directly captured at the protein level. By comparing with WT myotubes, we aimed to characterize

a disease signature of altered protein abundances in the F90I^{+/-} myotubes.

WT and F90I^{+/-} myotube cultures were treated with control morpholinos starting at day 4 in culture, replenished at day 7, and collected at day 10 for tandem mass tag (TMT) labeling and mass spectrometry. Using stringent criteria (false discovery rate of <0.01, coverage >10%, peptides >10) to ensure high confidence hits, we found 54 proteins with significantly altered abundances (log₂ fold change > 0.25 or < -0.25, p_{adj} < 0.05) between WT and F90I^{+/-} myotubes (Figure 2D, Table S1). Ontological analysis of these proteins supports their relevance to disease pathogenesis involving altered protein homeostasis and myofibrillar proteins (Figure 2E). We validated several of these changes via Western blot (Figures 2F, 2G and 4D). Consistent with the *in vitro* proteomic profile, we similarly found altered levels of proteins involved in myofibrillar structure and protein homeostasis in mature skeletal muscle from F90I^{+/-} mice (Figures 2H and 2I).

In parallel, WT myotubes were also treated with either BPAS or E8i8 morpholinos. While BPAS treatment had no appreciable impact on morphology, E8i8 seemed to negatively impact myotubes (Figures 3A and 3B). We also found treatment of WT myotubes with BPAS or E8i8 did not re-create the F90I^{+/-} proteomic profile (Figure 3C, Table S1). Although there was some overlap with the F90I^{+/-} disease profile (BPAS: 10/54 proteins; E8i8: 13/54 proteins), most of these changes were in the opposite direction of the F90I^{+/-} disease profile (BPAS: 6/10; E8i8: 9/13). BPAS treatment altered the abundance of a few proteins outside of the disease profile (10), whereas E8i8 treatment impacted far more (50) (Figure 3D, Table S1), likely reflecting the apparent morphological differences seen in E8i8-treated myotubes (Figures 3A and 3B).

We also treated F90I^{+/-} myotubes with morpholinos and again noticed that E8i8 but not BPAS had a negative impact on myotube morphology (Figures 4A and 4B). Because of E8i8's deleterious effect on myotubes and because the B isoform is thought to preferentially contribute to disease pathogenesis, we conducted mass spectrometry on BPAS-treated F90I^{+/-} myotubes and evaluated its impact on the proteomic disease signature.⁵ After treatment for 6 days, 31 of the 54 (57%) disease profile proteins returned to WT levels (Figure 4C). Western blot validation of heat shock protein (HSP)70, a protein directly linked to LGMDD1 pathogenesis, as well as DNAJB6b, confirmed a return to WT levels (Figures 4D–4F).⁸ Ontological analysis of proteins whose levels were corrected again involved categories related to protein homeostasis and myofibrillar proteins, whereas ontological analysis of those not corrected by BPAS treatment included many categories with no currently known connection to LGMDD1 pathogenesis (Figures 4G and 4H). Within the mouse transcriptome, BPAS's closest un-intended off-target sites had at least seven mismatches: *MAP3K3* (72% sequence complementarity), whereas off-target sites in the human transcriptome had at least nine mismatches: *ADGRG4* (64% sequence complementarity). *MAP3K3* abundances in our mouse proteomic dataset were not impacted by BPAS treatment (Table S1). Outside of the 54 disease

profile proteins, BPAS treatment did alter abundances of 46 other proteins (Figure 4I, Table S1), a majority of which are sarcomeric proteins, as shown by ontological analysis (Figure 4J). Although these 46 proteins did not meet significance criteria to be included in the disease profile, BPAS treatment shifted many of their abundances in the direction of WT levels (Figure 4I).

DISCUSSION

Since 2012, when mutations in *DNAJB6* were identified as a cause for dominantly inherited LGMD, there has been tremendous progress in the LGMDD1 field. Numerous cell and animal models have been generated, promising therapeutic targets are being identified, and outcome measures for future clinical trials are being defined.^{5,8,9,11} Despite this progress, there are no treatments for LGMDD1, and therapeutic target identification is still a significant need.

Previous studies have suggested the short B isoform of DNAJB6 preferentially contributes to LGMDD1 pathogenesis.^{5,6} This is supported by its localization to myofibrillar structures within skeletal muscle, a key site of pathology seen in human biopsies.^{6,15,16} Interestingly, the absence of both DNAJB6 isoforms is embryonic lethal in mice.⁴ While it is unknown if the postnatal absence of DNAJB6 is deleterious *in vivo*, therapeutic knockdown approaches for LGMDD1 that avoid complete DNAJB6 knockdown may have a wider therapeutic index.

Here we show the feasibility of DNAJB6 isoform-specific reduction and the potential of using morpholinos for LGMDD1 therapy via DNAJB6b knockdown. Although we did not experimentally compare the efficacy of different ASO chemistries, our choice to use morpholinos was influenced by the significant number of pre-clinical and clinical studies using morpholinos in neuromuscular disorders such as Duchenne muscular dystrophy and spinal muscular atrophy. Our study used morpholinos modified with an octaguanidine dendrimer to improve cellular uptake *in vitro* and *in vivo*. Although ideal for pre-clinical proof-of-principle studies, this form of morpholino has not been studied in human trials. Additionally, there are safety concerns related to fatal clotting episodes in mice treated with this modified morpholino.¹⁷ Future pre-clinical studies may use a more clinically translatable chemistry such as next-generation peptide-conjugated phosphorodiamidate morpholino oligomers (PMO), PMOs conjugated to TfR1-targeting antigen-binding fragments, or antibody-oligonucleotide conjugates. Another possible approach to achieve DNAJB6b isoform knockdown, with the added benefit of a single administration potentially providing lifelong treatment, is an adeno-associated virus (AAV) approach to deliver U7-small nuclear RNAs targeting the proximal PAS of *DNAJB6b*. AAV-delivered U7-snrRNAs are currently in clinical trials for Duchenne muscular dystrophy as an exon-skipping therapy for exon 2 duplications, and have been used pre-clinically in fascioscapulohumeral muscular dystrophy to decrease DUX4 expression by similarly targeting the PAS.^{18,19} However, given the uncertainty regarding the safety of long-term DNAJB6b isoform reduction, this AAV approach carries added risk.

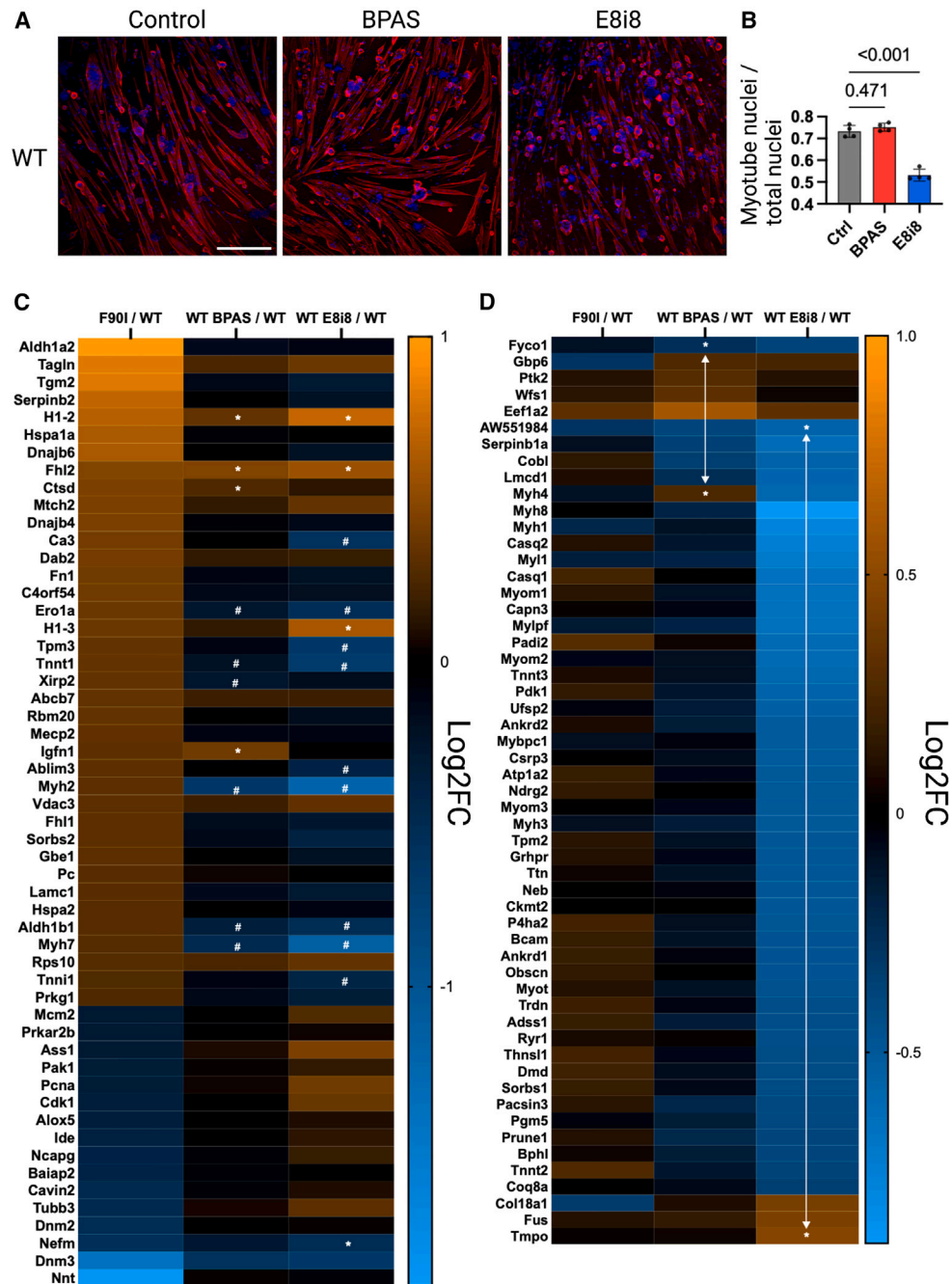


Figure 3. DNAJB6 isoform reduction does not mimic LGMDD1 proteomic signature

(A) WT primary myotubes at day 10 of differentiation and day 6 of treatment with control (5 μ m), BPAS (2.5 μ m), or E8i8 (5 μ m) morpholinos. Alpha-actinin (red) and DAPI (blue). Scale bar, 100 μ m. (B) Quantitation of myotube nuclei/total nuclei. Results presented as mean \pm SD. Dots represent experimental replicates (n = 4) two-tailed, unpaired Student's t test. (C) Heatmap of 54 proteins with altered abundance in F90I^{+/-} myotubes. Data expressed as log₂ fold change (log₂FC) relative to WT control treated myotubes. Higher abundance is indicated by orange, less abundance is represented by blue, and no change is black. Selective reduction of DNAJB6a (WT + BPAS) or DNAJB6a (WT + E8i8) do not re-create the proteomic pattern in F90I^{+/-} myotubes. Significant changes in the same direction as F90I^{+/-} (*). Significant changes in the opposite direction as F90I^{+/-} profile (#). Data are generated from three experimental replicates for control and BPAS treatment and two experimental replicates for E8i8 treatment. (D) Heatmap of proteins outside of the LGMDD1 proteomic signature whose abundances are altered by BPAS or E8i8 treatment. Data expressed as Log₂FC. Asterisks on the heatmap denote the proteins whose relative abundances were significantly altered by BPAS or E8i8 treatment.

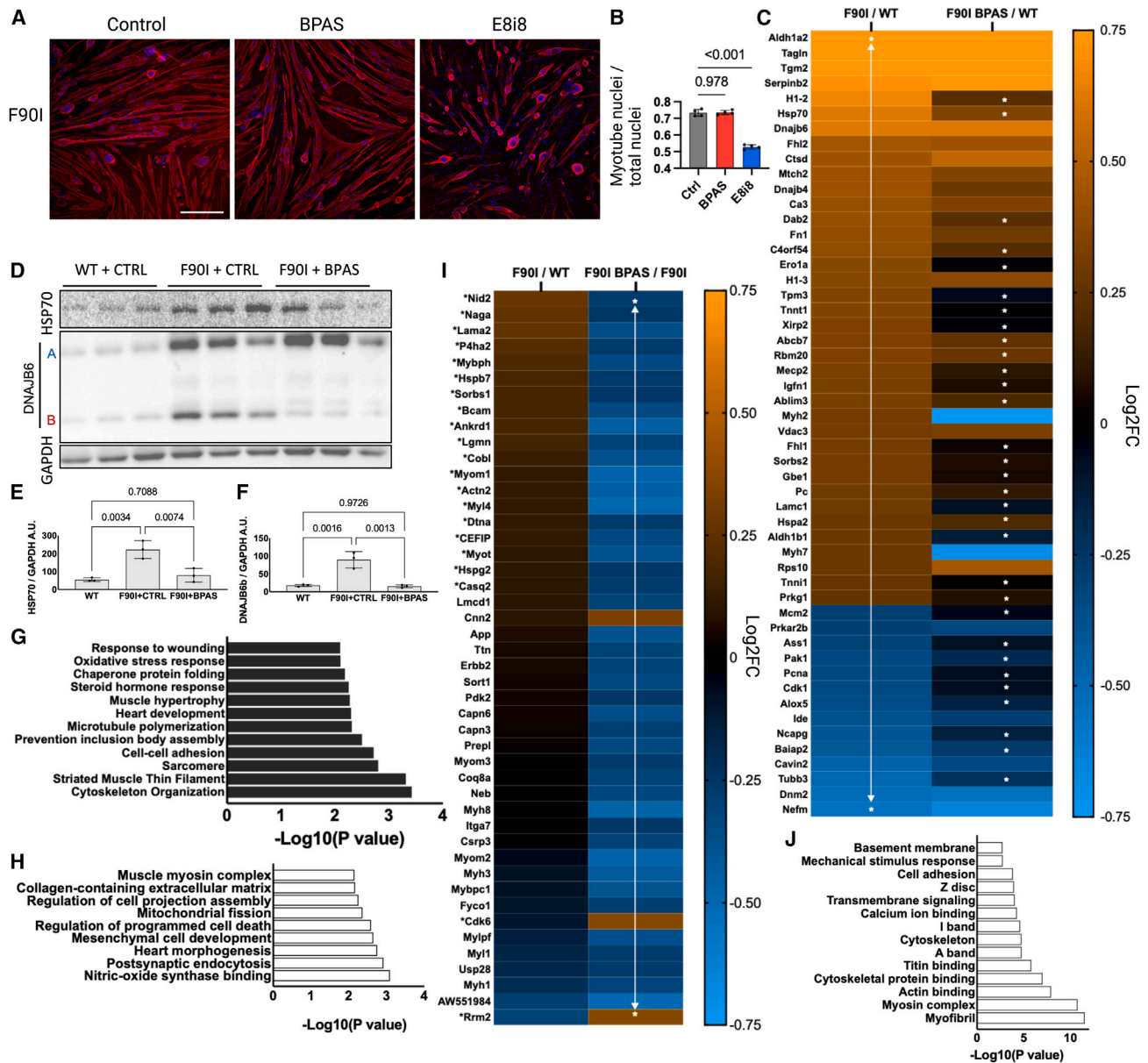


Figure 4. DNAJB6b isoform reduction partially normalizes proteomic signature in LGMDD1 primary mouse myotubes

(A) F90I^{+/-} primary myotubes at day 10 of differentiation, and day 6 of treatment with control (5 μ M), BPAS (2.5 μ M), or E8i8 (5 μ M) morpholinos. Alpha-actinin (red) and DAPI (blue). Scale bar, 100 μ m. (B) Quantitation of myotube nuclei/total nuclei. Results presented as mean \pm SD. Dots represent experimental replicates (n = 4) two-tailed, unpaired Student's t test. (C) Heatmap of 54 proteins with altered abundance in F90I^{+/-} myotubes. Data are expressed as log₂ fold change (log₂FC) relative to WT control-treated myotubes. Higher abundance is indicated by orange, less abundance is represented by blue, and no change is black. After BPAS treatment of F90I^{+/-} myotubes for 6 days, 31 of 54 proteins (57%) returned to WT levels. Asterisks denote the 31 proteins whose relative abundances were restored to WT levels (no significant difference compared to WT levels). Data are generated from three experimental replicates. (D) Western blot of myotube lysates from mass spectrometry experiment, validating HSP70 normalization after DNAJB6b reduction. (E) Quantitation of HSP70 western blot. Data presented as mean \pm SD. Dots represent experimental replicates (n = 3) from (D). (F) Quantitation of DNAJB6b Western blot. Data presented as mean \pm SD. Dots represent experimental replicates (n = 3) from (D). (G) Ontological analysis of 31 proteins corrected to WT levels with BPAS treatment. (H) Ontological analysis of proteins not corrected to WT levels with BPAS treatment. (I) Heatmap of proteins whose abundances are altered by BPAS treatment, outside of the 54-protein disease profile. Data are expressed as log₂FC. Higher abundance is indicated by orange, less abundance is represented by blue, and no change is black. Asterisks on the heatmap denote the proteins whose relative abundances were significantly altered by BPAS treatment. Proteins that did not meet significance requirements to be included in the proteomic disease profile, but BPAS treatment shifted their abundance toward WT levels, have asterisks next to their symbol. Data generated from three experimental replicates. (J) Ontological analysis of proteins outside of disease profiles that were significantly impacted by BPAS treatment.

Other than showing a decrease in DNAJB6 isoform levels at the RNA and protein levels in primary mouse myotube cultures and primary LGMDD1 patient-derived myoblasts, we demonstrated selective knockdown of DNAJB6 isoform protein levels in the TA muscle of mice with IM injections. We also provided preliminary evidence of safety against potential sequence specific off-target effects. Nucleotide BLAST results using BPAS's sequence against the mouse and human transcriptomes yielded no concerning hits with the closest targets having at least seven mismatches in mice and nine mismatches in humans. However, differences between the unintended mouse vs. human targets may result in different off-target effects, limiting the translatability of pre-clinical safety studies in mice.

Previous studies characterizing the mechanism regulating DNAJB6 isoform expression similarly used morpholinos to modify DNAJB6 isoform expression, but focused on reducing the A isoform, using a morpholino similar to E8i8.¹⁴ DNAJB6a is known to play a role in the replication cycle of several viruses, including HIV.²⁰ It was, therefore, hypothesized that the reduction of DNAJB6a could be a target for a broad-spectrum antiviral agent. Selective DNAJB6a reduction did in fact impair HIV and respiratory syncytial virus replication in human cell lines without any apparent negative effects.¹⁴ We observed a negative impact on both WT and F90I^{+/-} myotubes after DNAJB6a isoform knockdown. Importantly, a patient with a myofibrillar myopathy was recently reported to have homozygous recessive frameshift mutations selectively affecting the DNAJB6a isoform, resulting in the loss of A isoform protein expression.⁷ Additional work will need to clarify the mechanism behind these findings, as they raise concerns about the safety of interventions that greatly reduce DNAJB6a levels. We occasionally noticed an increase in DNAJB6a levels after treatment with BPAS (Figures 1C, 1F, 1K, 4D). While the mechanism for this observation remains unclear, it is possible that, by blocking the B isoform's PAS, the stronger distal PAS is preferentially used, shunting DNAJB6 mRNA production toward the A isoform. We also noted variability in the relative levels of each DNAJB6 isoform in myoblasts, myotubes, and mature skeletal muscle. Similar DNAJB6 isoform variability across different tissues has been described previously.²¹ Future research will also need to evaluate any risks associated with increased DNAJB6a levels, especially given its association with viral replication cycles and its role as a tumor suppressor.^{14,22-25}

Neither DNAJB6b nor DNAJB6a isoform reduction in WT myotubes mimicked the proteomic profile found in F90I^{+/-} myotubes. These findings need to be validated, but they suggest LGMDD1 pathogenesis cannot be explained by an isoform-specific loss of function. However, several other disease mechanisms could correlate with these results: a toxic gain of function, a dominant negative mechanism involving both isoforms, or a loss of function involving both isoforms. Repeating this mass spectrometry experiment and including non-isoform-specific knockdown of DNAJB6 could provide additional mechanistic insights.

Although the BPAS morpholino significantly decreased DNAJB6b levels, other sequences targeting DNAJB6's proximal PAS may be

more effective. Future work will aim to optimize the antisense sequence targeting this region. Alternate knockdown approaches, such as allele-specific knockdown, could similarly address the dominant disease mechanism of LGMDD1, while avoiding complete knockout. Our culture system of primary knockin LGMDD1 myotubes did not display any overt morphological abnormalities, but they do have a distinct, correctable, proteomic signature that was useful for screening therapeutics *in vitro*. Despite the notable variability in our Western blot validations (Figures 2F-2I), this pharmacoresponsive signature of altered protein homeostasis and myofibrillar proteins appears to extrapolate *in vivo* to our LGMDD1 mouse model. A proteomic signature obtained from human LGMDD1 myotubes and overlapped with that obtained in mice would further reinforce its relevance. Similar omics-based approaches are now commonly used to capture an unbiased disease signature, even in mild or pre-symptomatic disease stages, and then leveraged as a therapeutic biomarker.²⁶⁻²⁹

Our results suggest that DNAJB6b reduction may be beneficial in reversing the molecular effects of mutant DNAJB6 and improving a pathological *in vitro* phenotype. However, it remains unclear if reducing DNAJB6b levels is a viable approach for treating LGMDD1 patients. In fact, several aspects of this study suggest that such an approach may actually be harmful. Importantly, BPAS treatment altered the abundances of many other proteins outside of the LGMDD1 proteomic profile (Figure 4I). Even though BPAS treatment shifted many of these non-disease profile protein abundances toward WT levels, this finding raises concerns about the safety of DNAJB6b knockdown, even for short periods of time. As BPAS is not selective for the mutant allele, it is possible that BPAS treatment went beyond the potentially tolerated point of haploinsufficiency, in effect causing a loss of B-isoform function. This postnatal knockdown or absence of DNAJB6b may have long-term deleterious consequences in humans; DNAJB6b was recently found to be crucial for proper nuclear pore complex biogenesis.³⁰ Additionally, even DNAJB6 haploinsufficiency might have deleterious effects.¹³ Although human mutation databases contain frameshift and nonsense mutations scattered throughout DNAJB6, there seems to be a strong selection against loss-of-function variants based on gnomAD constraint metrics such as the probability of loss of function intolerance and the observed/expected ratio. It remains to be determined how much loss of expression can be safely tolerated while at the same time, how much reduction of the mutant allele is minimally required for benefit.

In conclusion, using primary LGMDD1 mouse myotubes, primary human LGMDD1 myoblasts, and skeletal muscle from a knockin LGMDD1 mouse model, we were able to show that our morpholinos could selectively reduce DNAJB6 isoforms. The functional effects of DNAJB6 isoform reduction on mature skeletal muscle and whether selective DNAJB6b reduction is a viable therapeutic target for LGMDD1 remains to be determined with a systemic treatment study in mice. These future studies will complement our *in vitro* findings, which show a limited view of both the benefit and potential harm

of DNAJB6b isoform reduction as a therapeutic approach for LGMD1. Additionally, we outline the use of an *in vitro*, therapeutically correctable proteomic disease signature in LGMD1 myotubes. Taken together, we expect these preliminary signs of both therapeutic benefit and possible harm from DNAJB6b reduction, and our unbiased proteomic method for screening therapeutics, to facilitate progress in the field toward production of effective and safe treatments for LGMD1.

MATERIALS AND METHODS

Morpholino treatment

Octaguanidine dendrimer-conjugated morpholino oligonucleotides (Gene Tools) were used in this study. BPAS (5'- TGCACCAAACA CATTGCGATTTATT-3'; Gene Tools), E8i8 (5'- CGTAGCAGGTG CTCCTTACCATTTA-3'; Gene Tools), A-PAS-1 (5'- ACATTTTAT TTACGTCAGTAGCACT-3'), A-PAS-2 (5'- AGACCTGCTTTTAT TTTTCATAGTA-3'), and negative control (5'-CCTCTTACCTCA GTTACAATTTATA-3'; Gene Tools). Morpholinos were added to cell culture media for the indicated time periods for each experiment. *In vitro* screening of morpholinos in primary mouse myotubes used doses of 2.5 μM , 5 μM , and 10 μM . To achieve more comparable levels of isoform-specific knockdown, primary mouse myotubes and primary human myoblasts were treated with 5 μM control, 5 μM E8i8, or 2.5 μM BPAS. This was due to BPAS having a more robust effect for a given dose. For *in vivo* treatments, after oxygen exposure, mice were anesthetized with isoflurane and injected intramuscularly (TA) with morpholinos (10 μg morpholino diluted in 20 μL PBS [Gibco]).

Primary mouse myoblast isolation and culture

Primary mouse myoblasts were isolated and cultured as previously described.³¹ At 2 months of age, WT and F90I^{+/-} mice were sacrificed, hindlimb muscles were isolated, and excess connective tissues and fat were cleaned in sterile PBS. Muscle tissues were minced into small pieces with scissors and added to a 50-mL conical tube with 1 mL of enzyme mix (500 U/mL type II collagenase [MP Biomed], 1.5 U/mL Collagenase D [Sigma], 2.5 U/mL Dispase II [Sigma], 2.5 mM CaCl₂, and PBS up to 1 mL). The mixture was shook at 37°C for 1 h, pelleted at 2,000 rpm for 5 min, and the supernatant was aspirated. The pellet was resuspended in proliferation medium (high-glucose DMEM [Gibco], supplemented with 20% fetal bovine serum [FBS, Gibco], 10% horse serum [HS, Remel], 0.5% chicken embryo extract [CEE, Accurate Chemical and Scientific], 2.5 ng/mL basic fibroblast growth factor [bFGF, PeproTech], 10 $\mu\text{g}/\text{mL}$ gentamycin, 1% anti-biotic/anti-mycotic [Gibco], and 2.5 $\mu\text{g}/\text{mL}$ Plasmocin prophylactic [Invivogen]), seeded on 10% Matrigel-coated dishes (45 $\mu\text{g}/\text{cm}^2$) at 10%–20% surface coverage, and incubated at 37°C and 10% CO₂. After cellular outgrowth from muscle explants was observed, tissues were transferred to new Matrigel-coated plates for additional rounds of myoblast outgrowth. Before confluence of cellular outgrowth, cells were detached using 0.25% trypsin and to improve myoblast purity, cells were pre-plated on collagen coated plates (type I rat tail collagen [Corning] in sterile water at 5 $\mu\text{g}/\text{cm}^2$) in growth medium, for 1 h at 37°C and 10%

CO₂. The supernatant was then transferred to Matrigel-coated dishes. Myoblasts were subsequently grown on Matrigel-coated dishes in proliferation medium, while cells on the collagen-coated plates were discarded. For myoblast differentiation, switching to a low serum media resulted in rapid myotube formation, contractions, and subsequent detachment. To avoid rapid detachment and facilitate slower differentiation and longer treatment with morpholinos, we plated myoblasts at a high baseline confluency in growth media, and infrequently changed the media to allow serum levels to be gradually consumed as myoblasts proliferate or differentiate into myotubes. The timing of media changes is detailed for each experiment.

Primary human myoblast isolation and culture

Healthy individuals and individuals with genetically confirmed LGMD1 were biopsied as part of ongoing research studies as approved by the Institutional Review Board of Washington University St. Louis (IRB# 202102146). Written informed consent was obtained according to the Declaration of Helsinki from all participants or a parent/legal guardian. Biopsies were performed at Washington University St. Louis by co-authors A.R.F. and C.C.W. TA core biopsies were obtained using sterile technique and equipment throughout the procedure. The skin overlying the biopsy site was marked and anesthetized with lidocaine. The co-axial introducer needle was inserted in the middle of the muscle belly. Three samples, totaling 45 mg, were collected from the TA with a micro-biopsy needle (Argon SuperCore Semi-Automatic Biopsy Instrument 14 G \times 9 cm, with 13 G \times 3.9 cm co-axial needle). After each pass, the semi-automatic biopsy instrument was removed from the co-axial introducer needle. Muscle samples were carefully removed and placed into vials with collection medium (Hanks' balanced salt solution [HBSS, Gibco], 1% penicillin-streptomycin (PS), and 0.25 $\mu\text{g}/\text{mL}$ amphotericin B).

Myoblasts were then isolated and cultured as previously described with minor modifications.^{31,32} Muscle was minced into small pieces using a McIlwain tissue chopper (Mickle Laboratory Engineering), added to a 15-mL conical tube with 1 mL of enzyme mix (1.5 U/mL Collagenase D, 2.5 U/mL Dispase II, 2.5 mM CaCl₂, HBSS up to 1 mL), and shook at 37°C for 1 h. Tissue fragments were pelleted at 2,000 rpm for 5 min and the supernatant was aspirated. The pellet was resuspended in human myoblast proliferation medium (20% FBS, 10% HS, 0.5% CEE, 2.5 ng/mL bFGF, 1% PS, 0.25 $\mu\text{g}/\text{mL}$ amphotericin), plated on 10% Matrigel-coated plates, and incubated at 37°C and 10% CO₂. After 2–3 days, the proliferation medium was replaced. Approximately 5 days later, when the muscle tissue is adherent and myoblast outgrowth is observed, but before cells become confluent, cells were detached using TrypLE express [Gibco], and pre-plated on collagen-coated plates for 1 h at 37°C at 10% CO₂. The supernatant was then transferred to 10% Matrigel-coated dishes (45 $\mu\text{g}/\text{cm}^2$) in human myoblast proliferation medium. Additional rounds of pre-plating (typically two rounds total) were performed as needed to enrich for cells with myoblast morphology. Myoblasts are grown in human myoblast proliferation medium until 85%–95% confluency

before switching to differentiation media (DMEM, 5% HS, 1% PS, 0.25 $\mu\text{g}/\text{mL}$ amphotericin B) to form myotubes. The medium is changed every 24–36 h.

Animal and experimental protocols

All animal experimental protocols were approved by the Animal Studies Committee of Washington University School of Medicine. CRISPR-Cas9-mediated knockin F901^{+/−} mice were generated as previously described, by the mouse genetics core facility for transgenic animal production at Washington University.⁸ Animal lines were bred on a C57/B6 background (The Jackson Laboratory) to at least the F5 generation. Control animals were F901^{−/−} littermates. Mice were housed in a temperature-controlled environment with 12-h light/12-h dark cycles, in which they received food and water ad libitum. Mice were euthanized, and skeletal muscle was dissected. For western blot, muscle was flash frozen in liquid nitrogen and stored at -80°C .

Immunofluorescence

Primary mouse myoblasts and myotubes were grown, stained, and imaged directly on cell culture plastic coated with 10% Matrigel. Primary human myotubes were grown, stained, and imaged on glass coverslips coated with 0.1% gelatin. All cells were washed three times with PBS, fixed in 4% paraformaldehyde for 10 min, permeabilized with 0.1% Triton X-100 in PBS for 10 min, and then blocked with 3% BSA in PBS for 30 min to 1 h at room temperature. Cells were stained with primary antibody (anti-rabbit alpha-actinin) at 4°C overnight, followed by washing three times with PBS. Cells were incubated with Alexa Fluor 555-conjugated secondary antibody at room temperature for 1 h and mounted with Mowiol media containing 4',6-diamidino-2-phenylindole (DAPI).

Differences between myotubes were quantitated as a ratio of nuclei within multinucleated alpha-actinin positive myotubes divided by the total number of nuclei. For each experimental replicate, nuclei were counted from five random fields taken with a $10\times$ objective equipped in a NIKON Eclipse 80i fluorescence microscope. For primary mouse myoblast cell count, myoblasts were plated at equal densities after quantification with a hemocytometer. For each time point, cells were stained with DAPI. Each experimental replicate was quantified as the average from five random fields. Individuals taking pictures and counting nuclei were blinded to genotype.

Western blot

Muscle tissues and cultured cells were homogenized using a radioimmunoprecipitation assay lysis buffer (50 mM Tris-HCl, pH 7.4, 150 mM NaCl, 1% NP-40, 0.25% Na-deoxycholate, and 1 mM EDTA) supplemented with protease inhibitor cocktail (Millipore Sigma), and lysates were centrifuged at 16,000g for 10 min. Protein concentrations were determined using a BCA Protein Assay Kit (ThermoFisher Scientific Inc.). Aliquots of unfractionated, total cell lysates were solubilized in Laemmli sample buffer, and equal amounts of proteins were separated on 12% SDS-PAGE gels. Proteins were transferred onto nitrocellulose membranes and then blocked with

5% nonfat dry milk in PBS with 0.1% Tween 20 for 1 h. The membrane was then incubated with primary antibodies, specific to the protein of interest, in 5% nonfat dry milk in PBS with 0.1% Tween overnight at 4°C . After incubation with the appropriate secondary antibody conjugated with horseradish peroxidase (HRP), ECL (GH Healthcare) was used for protein detection. Immunoblots were obtained using the G:Box Chemi XT4, Genesys, version 1.1.2.0 (SynGene). Densitometry was measured with ImageJ software (NIH).

Antibodies

The antibodies used were as follows: rabbit anti-GAPDH (Cell Signaling Technology; 2118), mouse anti-desmin (Dako; M0760), rabbit anti-DNAJB6 (Abcam; ab198995), mouse anti-HSP70 (Enzo Life Sciences; ADI-SPA-812) mouse anti-Synemin (Bioss, bs-8555R), rabbit anti-alpha Actinin (Abcam ab68167), rabbit anti-Cathepsin-D (Abcam, ab6313), mouse anti-myosin (Sigma, M1570), rabbit anti-DNAJB4 (Proteintech, 13064-1-AP), and rabbit anti-FHL2 (Abcam ab202584). The following secondary antibodies were used: anti-mouse IgG HRP (Cell Signaling Technology; 7076S), anti-rabbit IgG HRP (Cell Signaling Technology; 7074S), and anti-rabbit IgG (H + L) Alexa Fluor 555 (Invitrogen, ThermoFisher Scientific Inc.).

Real-time qPCR

Total RNA was isolated from primary myotubes with the SV Total RNA Isolation Kit (Promega; Z3100) according to the manufacturer's instructions. The concentration and quality of the total RNA isolated were determined using a NanoDrop spectrophotometer (ThermoFisher Scientific Inc.). cDNA was synthesized using the Transcriptor First-Strand cDNA Synthesis Kit with anchored oligo (dT)₁₈ primers (Roche; 04379012001). Gene expression levels were analyzed by real-time PCR on an Applied Biosystems model 7500 Software (version 2.0.5) using FastStart Universal SYBR Green Master ROX qPCR Mastermix (Roche; 04913850001). qPCR was performed with primers for *GAPDH* (F: ATGGTGAAGGTCGGTG TGA; R: AATCTCCACTTTGCCACTGC), *DNAJB6a* (F: TGGGTC TAAAAGCAACTGGG; R: AGTCCTCTTCTGCTTCTGC), and *DNAJB6b* (F: ACGACAAAGAGGATTGTGGAG; R: GCAGGTGCT CCTTACCATTTA). Values were normalized to GAPDH and are presented in log scale as $-\text{ddCT}$. Each data point (experimental replicate) was generated from three technical replicates.

TMT labeling proteomics

Primary myotubes were grown and treated with morpholinos as described above. Cell pellets were prepared for mass spectrometry acquisition by following the EasyPep Mini MS Sample Prep Kit (ThermoFisher Scientific Inc.). Peptide concentrations were determined with the Quantitative Fluorometric Peptide Assay (ThermoFisher Scientific Inc.). A total of 10 μg of peptide was prepared to label with TMTpro 16 plex reagents (ThermoFisher Scientific Inc.), according to the manufacturer's instructions. Labeled samples were combined and dried with vacuum centrifugation. Samples were then separated into eight fractions using the High pH Reversed-Phase Peptide Fractionation Kit (ThermoFisher Scientific

Inc.). The fractions were dissolved in 0.1% formic acid, and peptide concentrations were determined with Quantitative Colorimetric Peptide Assay (ThermoFisher Scientific Inc.). TMT-labeled sample liquid chromatography mass spectrometry acquisitions were performed using an EASY-nLC 1000 connected to an Orbitrap Eclipse Tribrid mass spectrometer (ThermoFisher Scientific Inc.). An amount of 0.5 µg of each fraction was loaded on an Aurora UHPLC Column (Ionopticks) and separated with a 136-min method, as described previously.³³ MS1 scans were acquired in the Orbitrap at 120 k resolution with a scan range of 350–1,800 m/z. The AGC target was 1×10^6 , and the maximum injection time was 50 ms. MS2 scans were acquired with higher-energy collisional dissociation activation type in the Orbitrap at 50 k resolution with the defined first mass 110 m/z. The isolation window was 0.5 m/z, collision energy was 38%, maximum injection time was dynamic, and AGC target was standard. System control and data collection were performed with Xcalibur software (ThermoFisher Scientific Inc.).

Proteomic analyses were performed with Proteome Discoverer 2.4 (ThermoFisher Scientific Inc.) using the Uniprot human database and the SequestHT with Percolator validation. TMTpro (Any N-Terminus) was set as a static N-Terminal Modification; TMTpro (K) and carbamidomethyl (C) were set as static modifications; oxidation (M) was set as a dynamic modification; acetyl (protein N-term), Met-loss (Protein N-term M), and Met-loss + acetyl (Protein N-term M) were set as dynamic N-terminal modifications. Normalization was performed relative to the total peptide amount. Further analyses were performed using the normalized abundance as below: limma analyses were performed using R studio following the user guide³⁴; volcano plots and heatmaps were generated with Prism 9.

Proteins were classified broadly into several catalogs according to the Gene Ontology (GO) annotation (geneontology.org). Overrepresentation analyses of GO terms, including biological process, molecular function, and cellular component, were performed using the ConsensusPathDB-human database system (cpdb.molgen.mpg.de/CPDB), which is a molecular functional interaction database. All proteins detected in the mass spectrometry experiments were used as background for comparison. A p value cutoff of 0.01 was selected.

Statistics

Comparisons between two groups were made using a two-tailed, unpaired Student's t test. Comparisons between several groups were made using either a one-way ANOVA with Tukey's post hoc test or two-way ANOVA with Bonferroni's post hoc test to adjust for multiple comparisons. All analyses were performed with GraphPad Prism 9 (GraphPad Software). Results were considered statistically significant if the p value was less than 0.05.

DATA AVAILABILITY

Qualified researchers may request access to the data that support the findings of this study from the corresponding author by contacting arfindlay@wustl.edu.

SUPPLEMENTAL INFORMATION

Supplemental information can be found online at <https://doi.org/10.1016/j.omtn.2023.05.017>.

ACKNOWLEDGMENTS

This work was supported by grants from the National Institute of Arthritis and Musculoskeletal and Skin Diseases (NIAMS): ARF (K08AR075894, R03AR081395), CCW (R01AR068797, K24AR073317); the American Society of Gene and Cell therapy (ASGCT): ARF (Career Development Award); the Children's Discovery Institute of Saint Louis Children's Hospital: ARF (Faculty Scholar Award-MIFR20221004); and the LGMD-1D DNAJB6 Foundation and International Registry (ARF). The graphical abstract was created with BioRender.

AUTHOR CONTRIBUTIONS

A.R.F.: conceptualization, formal analysis, funding acquisition, investigation, methodology, resources, supervision, validation, visualization, writing original draft, writing – review and editing. M.M.P., J.A.D., M.E.H., R.B., S.K.P., S.L., F.W., and T.C.: investigation, methodology. H.L.T. and T.M.M.: conceptualization, writing – review and editing. C.C.W.: conceptualization, funding acquisition, resources, supervision, validation, writing – review and editing.

DECLARATION OF INTERESTS

A.R.F. and C.C.W. are co-inventors on a pending patent application related to this publication (USPTO serial no. 17/932,996).

REFERENCES

- Findlay, A.R., Robinson, S.E., Poelker, S., Seiffert, M., Bengoechea, R., and Wehl, C.C. (2023). LGMDD1 natural history and phenotypic spectrum: implications for clinical trials. *Ann Clin Transl Neur* 10, 181–194. <https://doi.org/10.1002/acn3.51709>.
- Orlando, L. (2018). Genetic testing: MDA paves the way for better care in limb-girdle muscle weakness. *A Supplement to Neurology Reviews*, 51–54.
- Meng, E., Shevde, L.A., and Samant, R.S. (2016). Emerging roles and underlying molecular mechanisms of DNAJB6 in cancer. *Oncotarget* 7, 53984–53996. <https://doi.org/10.18632/oncotarget.9803>.
- Watson, E.D., Geary-Joo, C., Hughes, M., and Cross, J.C. (2007). The Mrj co-chaperone mediates keratin turnover and prevents the formation of toxic inclusion bodies in trophoblast cells of the placenta. *Development* 134, 1809–1817. <https://doi.org/10.1242/dev.02843>.
- Bengoechea, R., Pittman, S.K., Tuck, E.P., True, H.L., and Wehl, C.C. (2015). Myofibrillar disruption and RNA-binding protein aggregation in a mouse model of limb-girdle muscular dystrophy 1D. *Hum. Mol. Genet.* 24, 6588–6602. <https://doi.org/10.1093/hmg/ddv363>.
- Sarparanta, J., Jonson, P.H., Golzio, C., Sandell, S., Luque, H., Screen, M., McDonald, K., Stajich, J.M., Mahjneh, I., Vihola, A., et al. (2012). Mutations affecting the cytoplasmic functions of the co-chaperone DNAJB6 cause limb-girdle muscular dystrophy. *Nat. Genet.* 44, 450–455. <https://doi.org/10.1038/ng.1103>.
- Qian, F.-Y., Guo, Y.-D., Zu, J., Zhang, J.-H., Zheng, Y.-M., Abdoulaye, I.A., Pan, Z.-H., Xie, C.-M., Gao, H.-C., and Zhang, Z.-J. (2021). A novel recessive mutation affecting DNAJB6 causes myofibrillar myopathy. *Acta Neuropathol. Commun.* 9, 23. <https://doi.org/10.1186/s40478-020-01046-w>.
- Bengoechea, R., Findlay, A.R., Bhadra, A.K., Shao, H., Stein, K.C., Pittman, S.K., Daw, J.A., Gestwicki, J.E., True, H.L., and Wehl, C.C. (2020). Inhibition of DNAJ-HSP70 interaction improves strength in muscular dystrophy. *J. Clin. Invest.* 130, 4470–4485. <https://doi.org/10.1172/jci136167>.

9. Findlay, A.R., Bengoechea, R., Pittman, S.K., Chou, T.-F., True, H.L., and Wehl, C.C. (2019). Lithium chloride corrects weakness and myopathology in a preclinical model of LGMD1D. *Neurol. Genet.* 5, e318. <https://doi.org/10.1212/nxg.0000000000000318>.
10. Sarparanta, J., Jonson, P.H., Kawan, S., and Udd, B. (2020). Neuromuscular diseases due to chaperone mutations: a review and some new results. *Int. J. Mol. Sci.* 21, 1409. <https://doi.org/10.3390/ijms21041409>.
11. Stein, K.C., Bengoechea, R., Harms, M.B., Wehl, C.C., and True, H.L. (2014). Myopathy-causing mutations in an HSP40 chaperone disrupt processing of specific client conformers. *J. Biol. Chem.* 289, 21120–21130. <https://doi.org/10.1074/jbc.m114.572461>.
12. Bhadra, A.K., Rau, M.J., Daw, J.A., Fitzpatrick, J.A.J., Wehl, C.C., and True, H.L. (2022). Disease-associated mutations within the yeast DNAJB6 homolog Sisl slow conformer-specific substrate processing and can be corrected by the modulation of nucleotide exchange factors. *Nat. Commun.* 13, 4570. <https://doi.org/10.1038/s41467-022-32318-9>.
13. Ding, Y., Lang, D., Yan, J., Bu, H., Li, H., Jiao, K., Yang, J., Ni, H., Morotti, S., Le, T., et al. (2022). A phenotype-based forward genetic screen identifies Dnajb6 as a sick sinus syndrome gene. *Elife* 11, e77327. <https://doi.org/10.7554/elife.77327>.
14. Ko, S.-H., Liau, Y.-J., Chi, Y.-H., Lai, M.-J., Chiang, Y.-P., Lu, C.-Y., Chang, L.-Y., Tarn, W.-Y., and Huang, L.-M. (2019). Interference of DNAJB6/MRJ isoform switch by morpholino inhibits replication of HIV-1 and RSV. *Mol. Ther. Nucleic Acids* 14, 251–261. <https://doi.org/10.1016/j.omtn.2018.12.001>.
15. Harms, M.B., Sommerville, R.B., Allred, P., Bell, S., Ma, D., Cooper, P., Lopate, G., Pestronk, A., Wehl, C.C., and Baloh, R.H. (2012). Exome sequencing reveals DNAJB6 mutations in dominantly-inherited myopathy. *Ann. Neurol.* 71, 407–416. <https://doi.org/10.1002/ana.22683>.
16. Sandell, S., Huovinen, S., Palmio, J., Raheem, O., Lindfors, M., Zhao, F., Haapasalo, H., and Udd, B. (2016). Diagnostically important muscle pathology in DNAJB6 mutated LGMD1D. *Acta Neuropathol. Commun.* 4, 9. <https://doi.org/10.1186/s40478-016-0276-9>.
17. Ferguson, D.P., Dangott, L.J., and Lightfoot, J.T. (2014). Lessons learned from vivo-morpholinos: how to avoid vivo-morpholino toxicity. *Biotechniques* 56, 251–256. <https://doi.org/10.2144/000114167>.
18. Rashnonejad, A., Amini-Chermahini, G., Taylor, N.K., Wein, N., and Harper, S.Q. (2021). Designed U7 snRNAs inhibit DUX4 expression and improve FSHD-associated outcomes in DUX4 overexpressing cells and FSHD patient myotubes. *Mol. Ther. Nucleic Acids* 23, 476–486. <https://doi.org/10.1016/j.omtn.2020.12.004>.
19. Wein, N., Vetter, T.A., Vulin, A., Simmons, T.R., Frair, E.C., Bradley, A.J., Gushchina, L.V., Almeida, C.F., Huang, N., Lesman, D., et al. (2022). Systemic delivery of an AAV9 exon-skipping vector significantly improves or prevents features of Duchenne muscular dystrophy in the Dup2 mouse. *Mol. Ther. Methods Clin. Dev.* 26, 279–293. <https://doi.org/10.1016/j.omtm.2022.07.005>.
20. Chiang, Y.-P., Sheng, W.-H., Shao, P.-L., Chi, Y.-H., Chen, Y.-M.A., Huang, S.-W., Shih, H.-M., Chang, L.-Y., Lu, C.-Y., Chang, S.-C., et al. (2014). Large isoform of mammalian relative of DnaJ is a major determinant of human susceptibility to HIV-1 infection. *EBioMedicine* 1, 126–132. <https://doi.org/10.1016/j.ebiom.2014.10.002>.
21. Ding, Y., Long, P.A., Bos, J.M., Shih, Y.-H., Ma, X., Sundsbak, R.S., Chen, J., Jiang, Y., Zhao, L., Hu, X., et al. (2016). A modifier screen identifies DNAJB6 as a cardiomyopathy susceptibility gene. *Jci Insight* 1, e88797. <https://doi.org/10.1172/jci.insight.88797>.
22. Tagawa, S., Maringer, K., Li, X., Bernal-Rubio, D., Rauch, J.N., Gestwicki, J.E., Andino, R., Fernandez-Sesma, A., and Frydman, J. (2015). Defining Hsp70 subnetworks in dengue virus replication reveals key vulnerability in flavivirus infection. *Cell* 163, 1108–1123. <https://doi.org/10.1016/j.cell.2015.10.046>.
23. Cheng, X., Belshan, M., and Ratner, L. (2008). Hsp40 facilitates nuclear import of the human immunodeficiency virus type 2 vpx-mediated preintegration complex. *J. Virol.* 82, 1229–1237. <https://doi.org/10.1128/jvi.00540-07>.
24. Cao, Y.-Q., Yuan, L., Zhao, Q., Yuan, J.-L., Miao, C., Chang, Y.-F., Wen, X.-T., Wu, R., Huang, X.-B., Wen, Y.-P., et al. (2019). Hsp40 protein DNAJB6 interacts with viral NS3 and inhibits the replication of the Japanese encephalitis virus. *Int. J. Mol. Sci.* 20, 5719. <https://doi.org/10.3390/ijms20225719>.
25. Ko, S.-H., Huang, L.-M., and Tarn, W.-Y. (2019). The host heat shock protein MRJ/DNAJB6 modulates virus infection. *Front. Microbiol.* 10, 2885. <https://doi.org/10.3389/fmicb.2019.02885>.
26. Lim, K.R.Q., Maruyama, R., Echigoya, Y., Nguyen, Q., Zhang, A., Khawaja, H., Sen Chandra, S., Jones, T., Jones, P., Chen, Y.-W., and Yokota, T. (2020). Inhibition of DUX4 expression with antisense LNA gapmers as a therapy for facioscapulohumeral muscular dystrophy. *Proc. Natl. Acad. Sci. USA* 117, 16509–16515. <https://doi.org/10.1073/pnas.1909649117>.
27. Signorelli, M., Ebrahimipour, M., Veth, O., Hettne, K., Verwey, N., García-Rodríguez, R., Tanganyika-deWinter, C.L., Lopez Hernandez, L.B., Escobar Cedillo, R., Gómez Díaz, B., et al. (2021). Peripheral blood transcriptome profiling enables monitoring disease progression in dystrophic mice and patients. *EMBO Mol. Med.* 13, e13328. <https://doi.org/10.15252/emmm.202013328>.
28. Capitanio, D., Moriggi, M., Torretta, E., Barbacini, P., De Palma, S., Viganò, A., Lochmüller, H., Muntoni, F., Ferlini, A., Mora, M., and Gelfi, C. (2020). Comparative proteomic analyses of Duchenne muscular dystrophy and Becker muscular dystrophy muscles: changes contributing to preserve muscle function in Becker muscular dystrophy patients. *J. Cachexia Sarcopenia Muscle* 11, 547–563. <https://doi.org/10.1002/jcsm.12527>.
29. Walsh, C.J., Batt, J., Herridge, M.S., Mathur, S., Bader, G.D., Hu, P., Khatri, P., and Dos Santos, C.C. (2022). Comprehensive multi-cohort transcriptional meta-analysis of muscle diseases identifies a signature of disease severity. *Sci. Rep.* 12, 11260. <https://doi.org/10.1038/s41598-022-15003-1>.
30. Kuiper, E.F.E., Gallardo, P., Bergsma, T., Mari, M., Kolbe Musskopf, M., Kuipers, J., Giepmans, B.N.G., Steen, A., Kampinga, H.H., Veenhoff, L.M., and Bergink, S. (2022). The chaperone DNAJB6 surveils FG-nucleoporins and is required for interphase nuclear pore complex biogenesis. *Nat. Cell Biol.* 24, 1584–1594. <https://doi.org/10.1038/s41556-022-01010-x>.
31. Shahini, A., Vydiam, K., Choudhury, D., Rajabian, N., Nguyen, T., Lei, P., and Andreadis, S.T. (2018). Efficient and high yield isolation of myoblasts from skeletal muscle. *Stem Cell Res.* 30, 122–129. <https://doi.org/10.1016/j.scr.2018.05.017>.
32. Spinazzola, J.M., and Gussoni, E. (2017). Isolation of primary human skeletal muscle cells. *Bio. Protoc.* 7, e2591. <https://doi.org/10.21769/bioprotoc.2591>.
33. Zhang, G., Li, S., Wang, F., Jones, A.C., Goldberg, A.F.G., Lin, B., Virgil, S., Stoltz, B.M., Deshaies, R.J., and Chou, T.-F. (2021). A covalent p97/VCP ATPase inhibitor can overcome resistance to CB-5083 and NMS-873 in colorectal cancer cells. *Eur. J. Med. Chem.* 213, 113148. <https://doi.org/10.1016/j.ejmech.2020.113148>.
34. Ritchie, M.E., Phipson, B., Wu, D., Hu, Y., Law, C.W., Shi, W., and Smyth, G.K. (2015). Limma powers differential expression analyses for RNA-seq and microarray studies. *Nucleic Acids Res.* 43, e47. <https://doi.org/10.1093/nar/gkv007>.